

000 HIERARCHICAL SEMANTIC-ACOUSTIC MODELING 001 VIA SEMI-DISCRETE RESIDUAL REPRESENTATIONS 002 FOR EXPRESSIVE END-TO-END SPEECH SYNTHESIS 003 004

006 **Anonymous authors**

007 Paper under double-blind review

011 ABSTRACT

013 Generative models for speech synthesis face a fundamental trade-off: discrete
014 tokens ensure stability but sacrifice expressivity, while continuous signals retain
015 acoustic richness but suffer from error accumulation due to task entanglement.
016 This challenge has driven the field towards multi-stage pipelines that rely on pre-
017 trained **discrete** speech tokenizers, but these create a semantic-acoustic divide,
018 limiting holistic and expressive speech generation. We resolve these dilemma
019 through hierarchical semantic-acoustic modeling with semi-discrete residual rep-
020 resentations. Our framework introduces a differentiable quantization bottleneck
021 that induces natural specialization: a Text-Semantic Language Model (TSLM)
022 generates semantic-prosodic plans, while a Residual Acoustic Model (RALM)
023 recovers fine-grained acoustic details. This hierarchical semantic-acoustic repre-
024 sentation guides a local diffusion-based decoder to generate high-fidelity speech
025 latents. Critically, the entire architecture is trained end-to-end under a simple dif-
026 fusion objective, eliminating dependency on external **discrete** speech tokenizers.
027 Trained on over 1 million hours of speech, our 0.5B-parameter model achieves
028 state-of-the-art zero-shot TTS performance among open-source systems, demon-
029 strating that our approach delivers expressive and stable synthesis. Audio samples
030 are available at: <https://voxcpm.github.io/VoxCPM-demopage/>.

031 1 INTRODUCTION

033 The pursuit of modern text-to-speech (TTS) systems has evolved beyond intelligibility toward the
034 synthesis of genuinely human-like audio, capable of conveying subtle emotions, speaker identity,
035 and contextual nuances (Shen et al., 2018; Ping et al., 2017; Ren et al., 2020; Li et al., 2019). This
036 leap is critical for applications like empathetic virtual assistants and immersive digital avatars, and
037 hinges on a core technical challenge: simultaneously capturing the fine-grained acoustic details that
038 define vocal richness and the long-range semantic structures governing intelligibility and natural
039 prosody.

040 Inspired by the success of large language models (LLMs), a dominant paradigm frames TTS as a
041 sequence modeling task over discrete tokens from pre-trained neural audio codecs (e.g., EnCodec
042 (Défossez et al., 2022)). Autoregressively or Non-autoregressively predicting these tokens from text
043 or phonemes (Borsos et al., 2023a; Kharitonov et al., 2023; Chen et al., 2025; Wang et al., 2025c;
044 Peng et al., 2024) offers excellent scalability and in-context learning capabilities. However, this
045 approach faces a fundamental “quantization ceiling”, as the compression process irreversibly dis-
046 cards subtle acoustic details. To mitigate this quality loss, state-of-the-art TTS systems (Du et al.,
047 2024a;b; 2025; Zhou et al., 2025; Casanova et al., 2024) adopt multi-stage hybrid pipelines. Here, an
048 LLM generates discrete tokens which condition a separate diffusion-based decoder. While improv-
049 ing fidelity, this solution creates a stark semantic-acoustic divide: the LLM operates in an abstract,
050 discrete space unaware of acoustic reality, while the diffusion model performs local refinement with-
051 out high-level context. This fragmentation prevents end-to-end optimization and limits holistic and
052 expressive speech synthesis.

053 Alternatively, other approaches directly model continuous speech representations to avoid quan-
054 tization loss. Early systems like Tacotron 2 (Shen et al., 2018) and more recent models such as

MELLE (Meng et al., 2024) generate mel-spectrograms autoregressively. However, predicting continuous targets under standard regression losses often yields over-smoothed and low-diversity outputs. To address this, recent innovations have explored replacing the regression objective with a denoising process to model the distribution of the next continuous representations, spanning both non-autoregressive paradigms (Shen et al., 2023; Le et al., 2023; Chen et al., 2024) and autoregressive methods (Li et al., 2024; Jia et al., 2025; Peng et al., 2025). Among these, autoregressive approaches have often demonstrated superior performance in capturing natural prosody and expressive variation. This innovation successfully enhances the detail and diversity of generated continuous representations. However, a more fundamental issue persists: in a fully continuous autoregressive model, the tasks of high-level semantic-prosodic planning and fine-grained acoustic rendering are conflated within a single learning objective. The model is forced to simultaneously solve two disparate tasks—requiring different inductive biases—in a continuous output space. This entanglement presents a significant challenge to the modeling capacity of a single LLM, as it must learn to be both a global planner and a local renderer without an inherent architectural bias to separate these functions. We argue that this conflation is a root cause of instability. The model’s focus is inevitably pulled towards fitting low-level acoustic textures, which compromises its ability to maintain high-level semantic coherence, leading to the well-known problem of error accumulation over long sequences (Pasini et al., 2024).

In this work, we introduce a unified, end-to-end framework that resolves this trade-off through hierarchical semantic-acoustic modeling with semi-discrete residual representations. Our key insight is that holistic and expressive speech synthesis requires explicit architectural separation between semantic-prosodic planning and acoustic rendering, yet should remain within a cohesive, end-to-end trainable system. The core innovation is a differentiable Finite Scalar Quantization (FSQ) (Mentzer et al., 2024) bottleneck that induces natural specialization: (1) a Text-Semantic Language Model (TSLM) generates semantic-prosodic plans stabilized through quantization, focusing on linguistically meaningful patterns; and (2) a Residual Acoustic Language Model (RALM) recovers fine-grained details lost during quantization, specializing in acoustic refinement. This hierarchical design enables each component to excel at its respective role while maintaining differentiability, and both of them will be used to guide a local diffusion decoder to generate high-fidelity speech latents. Critically, the entire hierarchical model is trained end-to-end under a simple diffusion objective, seamlessly integrating planning and rendering without pre-trained tokenizers. Our main contributions are as follows.

- We propose an end-to-end hierarchical architecture that introduces an internal semi-discrete bottleneck to resolve the expressivity-stability trade-off. This mechanism implicitly addresses task entanglement in continuous models by inducing a beneficial separation between semantic-prosodic planning and fine-grained acoustic modeling within a single, unified framework.
- We introduce a residual learning strategy that, in conjunction with the bottleneck, enables a holistic yet specialized modeling process. Unlike fragmented multi-stage pipelines, our approach achieves functional separation without architectural fragmentation, simplifying the training pipeline and eliminating dependency on external *discrete* speech tokenizers.
- We demonstrate the efficacy of our approach through large-scale training on over 1 million hours of bilingual speech. The resulting model, VoxCPM-0.5B, achieves state-of-the-art zero-shot TTS performance among open-source systems, validating its practical strength.
- We provide extensive ablation studies that conclusively validate the semi-discrete residual representations as the crucial component for robust, expressive, and long-form synthesis. We will release code and models to support future research.

2 RELATED WORK

2.1 DISCRETE TOKEN-BASED TTS

The discrete token paradigm has emerged as a dominant approach in modern TTS, leveraging the success of large language models. This method converts speech into discrete representations using neural audio codecs such as EnCodec (Défossez et al., 2022) and DAC (Kumar et al., 2023) through residual vector quantization (RVQ). AudioLM (Borsos et al., 2023a) and VALL-E (Chen et al., 2025) pioneered this direction by framing TTS as an autoregressive sequence prediction task over discrete acoustic tokens. Subsequent developments include SoundStorm (Borsos et al., 2023b), which in-

108 introduced non-autoregressive generation for improved efficiency, and Spear-TTS (Kharitonov et al.,
 109 2023), which focused on multilingual capabilities with minimum supervision.
 110

111 Recent advancements have focused on enhancing the scalability, controllability and zero-shot adap-
 112 tation. CosyVoice (Du et al., 2024a) proposed supervised semantic tokens for improved zero-shot
 113 performance, while its successors, CosyVoice 2 and 3 (Du et al., 2024b; 2025) incorporated text-
 114 based LLM initialization and streaming synthesis for human-parity quality and low latency. In-
 115 dexTTS (Deng et al., 2025) and IndexTTS2 (Zhou et al., 2025) introduced precise duration and
 116 emotion control in autoregressive token generation, enabling applications with strict timing and ex-
 117 pressivity requirements. SparkTTS (Wang et al., 2025b) utilized single-stream decoupled speech to-
 118 kens for modeling efficiency, and FireRedTTS (Guo et al., 2024) along with its update FireRedTTS-2
 119 (Xie et al., 2025) established frameworks for industry-level generative speech, including long-form
 120 multi-speaker dialogue. Despite these progresses, discrete approaches suffer from inherent quanti-
 121 zation artifacts, limiting acoustic fidelity and prompting hybrid solutions.
 122

2.2 CONTINUOUS REPRESENTATION TTS

123 To circumvent quantization losses in discrete models, continuous representation approaches directly
 124 model speech features such as mel-spectrograms or audio latents. Early systems like Tacotron 2
 125 (Shen et al., 2018) established the encoder-decoder framework for text-to-mel mapping, while Fast-
 126 Speech (Ren et al., 2020) introduced explicit duration modeling for alignment stability. Recent de-
 127 velopments have integrated diffusion processes to enhance detail and diversity. Non-autoregressive
 128 models like NaturalSpeech 2 (Shen et al., 2023) and VoiceBox (Le et al., 2023) apply diffusion
 129 directly on continuous representations. F5-TTS (Chen et al., 2024) advanced flow-matching for effi-
 130 cient synthesis. Autoregressive paradigms, often superior in prosody and variation, include MELLE
 131 (Meng et al., 2024) for mel-spectrogram generation. Innovations like ARDiT (Li et al., 2024) use
 132 an autoregressive diffusion transformer for TTS, unifying semantic coherence and acoustic natural-
 133 ness via parameter sharing. DiTAR (Jia et al., 2025) extended this with a patch-based design: a
 134 causal LM for inter-patch stability and a bidirectional local diffusion transformer for intra-patch re-
 135 finement. VibeVoice (Peng et al., 2025) employed next-token diffusion for long-form multi-speaker
 136 synthesis. More recent models such as CLEAR (Wu et al., 2025) and FELLE (Wang et al., 2025a)
 137 focus on latent autoregressive modeling with token-wise coarse-to-fine hierarchies, while MELA-
 138 TTS (An et al., 2025) and KALL-E (Zhu et al., 2024) combine joint transformer-diffusion with
 139 next-distribution prediction for improved efficiency and quality. Despite these advances, continuous
 140 models often entangle high-level semantic planning with low-level acoustic rendering, leading to
 141 instability in long sequences without explicit separation.
 142

2.3 HIERARCHICAL AND RESIDUAL MODELING IN TTS

143 Hierarchical and residual approaches decompose TTS into layered tasks to balance stability and ex-
 144 pressivity. HierSpeech++ (Lee et al., 2025) employed variational inference for semantic-acoustic
 145 mapping. HALL-E (Nishimura et al., 2025) uses hierarchical neural codecs with LLMs for minute-
 146 long synthesis. MARS6 (Baas et al., 2025) builds robust encoder-decoder transformers with hierar-
 147 chical tokens. DiffStyleTTS (Liu et al., 2024) applies diffusion for hierarchical prosody modeling.
 148 HAM-TTS (Wang et al., 2024) introduces hierarchical acoustic modeling with data augmentation
 149 for zero-shot TTS. QTTS (Han et al., 2025) features hierarchical parallel architectures for residu-
 150 ally quantized codes. These methods address flaws in prior paradigms: implicit designs lack regu-
 151 lated bottlenecks, tokenizer-dependent models suffer discrete losses, and fragmented stages hinder
 152 end-to-end optimization. However, few fully integrate explicit residual designs with semi-discrete
 153 bottlenecks in a unified framework, as proposed in our work, to achieve implicit disentanglement
 154 without external dependencies.
 155

3 METHODOLOGY

3.1 CORE DESIGN MOTIVATION

158 Generative speech synthesis faces a fundamental tension between expressivity and stability. Dis-
 159 crete tokenization methods (e.g., [discrete](#) speech tokenizers with language models) ensure stable
 160 autoregressive generation but irreversibly discard fine-grained acoustic details through quantization.
 161

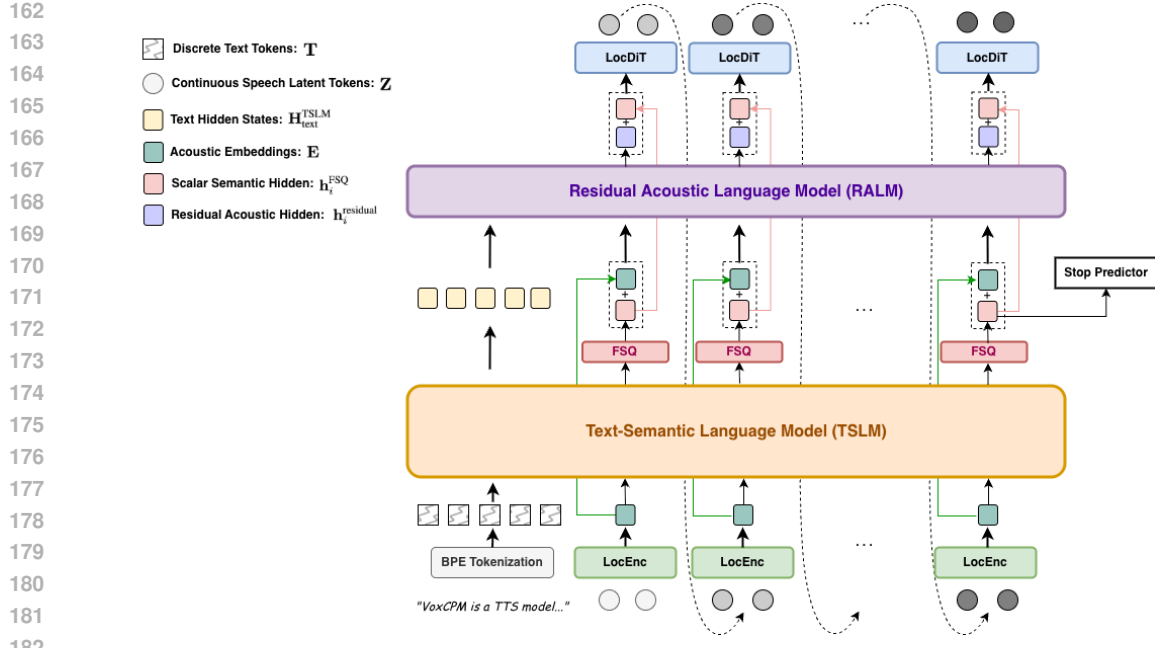


Figure 1: Overall architecture of VoxCPM. The model hierarchically generates speech by first processing audio latents through a LocEnc, then producing a semi-discrete speech skeleton with the TSLM and FSQ, refining acoustic details with the RALM, and finally generating high-fidelity latent output with the LocDiT.

Continuous approaches preserve full fidelity but suffer from error accumulation in long sequences due to information entanglement, often leading to catastrophic failure in intelligibility.

Critically, we identify a key limitation in existing discrete tokenization approaches: methods that directly use FSQ or VQ to obtain discrete codebooks for language modeling face an inherent scalability challenge. As the dimensionality increases to capture richer acoustic information, the codebook size grows exponentially, creating an unmanageably large and sparse vocabulary that language models struggle to predict accurately.

We hypothesize that an effective solution should **structurally separate** the modeling of stable semantic-prosodic content from fine-grained acoustic details while maintaining differentiability for end-to-end training. Our key insight is to introduce a **differentiable quantization bottleneck** that naturally induces this separation through scalar quantization, splitting information into a discrete-like skeleton for content stability and continuous residual components for detail expressivity.

Unlike multi-stage TTS systems composed of separate LM and diffusion that treat quantization as a means to obtain discrete prediction targets, our approach uses quantization solely as a regularization mechanism to constrain the hidden state space. This distinction allows us to avoid the vocabulary explosion problem while still benefiting from the stabilizing effects of discrete representations.

3.2 MODEL OVERVIEW

VoxCPM employs a hierarchical autoregressive architecture that generates sequences of continuous speech latents $\mathbf{Z} = \{\mathbf{z}_1, \dots, \mathbf{z}_M\}$ conditioned on input text tokens $\mathbf{T} = \{t_1, \dots, t_N\}$, where each $\mathbf{z}_i \in \mathbb{R}^{P \times D}$ represents a patch of P frames with D -dimensional VAE latent vectors. The generation process follows:

$$p(\mathbf{Z}|\mathbf{T}) = \prod_{i=1}^M p(\mathbf{z}_i|\mathbf{T}, \mathbf{Z}_{<i}) \quad (1)$$

The core innovation lies in our hierarchical conditioning mechanism with residual representation learning. It is made up of a local audio encoder (LocEnc), a text-semantic language model (TSLM),

216 a residual acoustic language model (RALM) and a local diffusion transformer decoder (LocDiT). A
 217 stop predictor is attached to the output of the TSLM to determine the endpoint of generation. As
 218 shown in Figure 1, each patch generation involves:
 219

$$220 \quad \mathbf{z}_i \sim \text{LocDiT}(\mathbf{h}_i^{\text{final}}), \quad \mathbf{h}_i^{\text{final}} = \underbrace{\text{FSQ}(\text{TSLM}(\mathbf{T}, \mathbf{E}_{<i}))}_{\text{stable skeleton}} + \underbrace{\text{RALM}(\cdot)}_{\text{residual details}} \quad (2)$$

$$221$$

$$222$$

223 where $\mathbf{E}_{<i} = \text{LocEnc}(\mathbf{Z}_{<i})$ represents historical audio context aggregated by a lightweight LocEnc
 224 that compresses VAE latent patches into compact acoustic embeddings. The hierarchical backbone
 225 produces a conditioning signal $\mathbf{h}_i^{\text{final}}$ that encapsulates both semantic content from TSLM (with FSQ)
 226 and acoustic details from RALM. This signal guides the LocDiT to generate the current latent patch
 227 \mathbf{z}_i through a denoising diffusion process. The entire model is trained end-to-end with gradients flowing
 228 through all components, including the FSQ bottleneck via straight-through estimation, ensuring
 229 coordinated optimization toward holistic speech synthesis.
 230

231 3.3 HIERARCHICAL SEMANTIC-ACOUSTIC MODELING

232 Our hierarchical modeling approach is designed to implicitly separate semantic-prosodic planning
 233 from fine-grained acoustic synthesis, addressing the fundamental stability-expressivity trade-off
 234 through structured representation learning.
 235

236 3.3.1 TEXT-SEMANTIC LANGUAGE MODEL (TSLM)

237 The Text-Semantic Language Model forms the main part of our hierarchical architecture, responsible
 238 for capturing high-level linguistic structure and generating contextually appropriate speech patterns.
 239 Unlike conventional TTS systems that typically operate on phoneme sequences, our approach
 240 leverages a pre-trained text language model (MiniCPM-4 (Team et al., 2025)) as its initial backbone,
 241 enabling richer contextual understanding and more natural prosody prediction directly from
 242 raw text. By processing both text tokens and historical audio context, the TSLM learns to generate
 243 semantic content and prosodic structure that evolve naturally throughout an utterance, reflecting
 244 the underlying linguistic meaning rather than simply mapping phonemes to acoustic features. The
 245 TSLM produces continuous semantic-prosodic representations that encode both the content to be
 246 spoken and how it should be prosodically realized, serving as input to the subsequent quantization
 247 stage.
 248

249 3.3.2 SEMI-DISCRETE REPRESENTATION LEARNING VIA FSQ

250 At the core of our approach lies the Finite Scalar Quantization (FSQ) layer, which projects the continuous hidden states from the TSLM onto a structured lattice to create a semi-discrete representation.
 251 The FSQ operation transforms each dimension of the continuous vector through a deterministic
 252 scalar quantization:
 253

$$254 \quad \mathbf{h}_{i,j}^{\text{FSQ}} = \Delta \cdot \text{clip} \left(\text{round} \left(\frac{\mathbf{h}_{i,j}^{\text{TSLM}}}{\Delta} \right), -L, L \right) \quad (3)$$

$$255$$

$$256$$

$$257$$

258 where Δ is the quantization step size, L is the clipping range, and round maps values to discrete
 259 levels. This transformation creates a structured discrete representation while maintaining differentiability
 260 through the straight-through estimator during backward passes.
 261

262 The FSQ layer acts as a bottleneck, analogous to the first layer of Residual Vector Quantization
 263 (RVQ), which captures a coarse semantic-prosodic skeleton (e.g., content, intonation patterns). We
 264 term this representation “semi-discrete” as it employs a significantly larger dimensionality than standard
 265 FSQ to ensure sufficient informational capacity. Unlike RVQ, where the first layer is a prediction
 266 target and subsequent layers model finer details, our FSQ bottleneck serves as an intermediate,
 267 differentiable inductive bias within the continuous data flow. It encourages the model to prioritize
 268 modeling stable, high-level components (the semantic-prosodic skeleton) by providing a clear
 269 learning signal for what information should be preserved through the bottleneck. This structured
 270 approach mitigates error accumulation by reducing the modeling burden on the TSLM, allowing it
 271 to focus on the major components of the speech.
 272

270 3.3.3 RESIDUAL ACOUSTIC MODELING
271

272 To recover the fine-grained acoustic information attenuated by quantization, we introduce the Residual
273 Acoustic Language Model (RALM). This module specializes in reconstructing those subtle vocal
274 characteristics that conventional discrete methods sacrifice for stability. It processes the quantization
275 residuals along with contextual information to recover speaker identity, spectral fine structure, and
276 micro-prosodic variations:

$$277 \quad \mathbf{h}_i^{\text{residual}} = \text{RALM}(\mathbf{H}_{\text{text}}^{\text{TSLM}}, \mathbf{H}_{<i}^{\text{FSQ}} \oplus \mathbf{E}_{<i}) \quad (4)$$

279 Here, the RALM conditions its predictions on both the TSLM hidden states of the text part $\mathbf{H}_{\text{text}}^{\text{TSLM}}$,
280 the semi-discrete representation of speech part $\mathbf{H}_{<i}^{\text{FSQ}}$, and the historical acoustic embeddings $\mathbf{E}_{<i}$.
281 This residual learning approach creates a natural division of labor: the TSLM+FSQ pathway fo-
282 cuses on content stability and prosodic coherence, while the RALM pathway specializes in acoustic
283 expressivity and speaker characteristics.

284 The final combined representation $\mathbf{h}_i^{\text{final}} = \mathbf{h}_i^{\text{FSQ}} + \mathbf{h}_i^{\text{residual}}$ thus encapsulates both semantic stability
285 and acoustic expressivity, creating a comprehensive signal that guides the subsequent local diffusion
286 process.

288 3.3.4 LOCAL DIFFUSION TRANSFORMER DECODER
289

290 The Local Diffusion Transformer (LocDiT) serves as our high-fidelity synthesis module, generat-
291 ing continuous latent patches conditioned on the hierarchical representation $\mathbf{h}_i^{\text{final}}$ produced by the
292 preceding modules. Following DiTAR (Jia et al., 2025), we employ a bidirectional Transformer
293 architecture that enables full receptive field modeling within each patch. To enhance generation
294 consistency, we incorporate the previous patch \mathbf{z}_{i-1} as additional conditioning context, which has
295 been empirically validated to significantly improve output quality by framing the task as outpainting
296 rather than independent patch generation. Besides, we mask the LM guidance in LocDiT condition
297 with a specific probability ratio, for enabling classifier-free guidance (CFG) during inference.

298 3.4 TRAINING OBJECTIVE
299

300 The entire model is trained end-to-end using a flow-matching objective that directly optimizes the
301 quality of the generated speech latents. We adopt the conditional flow-matching formulation for its
302 training stability and sampling efficiency:

$$303 \quad \mathcal{L}_{\text{FM}} = \mathbb{E}_{t, \mathbf{z}_i^0, \epsilon} \left[|\mathbf{v}_\theta(\mathbf{z}_i^t, t, \mathbf{h}_i^{\text{final}}, \mathbf{z}_{i-1}) - \frac{d}{dt}(\alpha_t \mathbf{z}_i^0 + \sigma_t \epsilon)|^2 \right] \quad (5)$$

306 where $\mathbf{z}_i^t = \alpha_t \mathbf{z}_i^0 + \sigma_t \epsilon$ is the noisy latent at time t , with $\epsilon \sim \mathcal{N}(0, I)$, and \mathbf{v}_θ is the velocity field
307 predicted by the LocDiT.

308 **Simultaneously, a binary classification loss is applied to train the model to predict the end of a speech
309 sequence:**

$$310 \quad \mathcal{L}_{\text{Stop}} = \mathbb{E}_{i \sim \text{sequence}} \left[\text{BCE} \left(s_\theta(\mathbf{h}_i^{\text{FSQ}}), \mathbb{1}[\text{token } i \text{ is the last}] \right) \right] \quad (6)$$

312 where s_θ is a stop-logit projection layer, and BCE denotes the binary cross-entropy loss.

313 The gradients from this loss are backpropagated through the entire autoregressive hierarchy, includ-
314 ing the FSQ layer (via straight-through estimation), the TSLM and the LocEnc. This end-to-end
315 optimization under the combined objective $\mathcal{L} = \mathcal{L}_{\text{FM}} + \lambda \mathcal{L}_{\text{Stop}}$ allows each component to learn its
316 specialized role—semantic planning, stabilization, and acoustic refinement—in a coordinated man-
317 ner, guided by the unified objective of accurately modeling the continuous speech latents.

319 3.5 CAUSAL AUDIO VAE
320

321 To enable efficient streaming synthesis, we employ a causal Variational Autoencoder that operates in
322 a computationally efficient latent space. VAE is pre-trained separately using a composite objective
323 that combines reconstruction loss in the Mel-spectrogram domain, adversarial training with multi-
period and multi-scale discriminators, and a minimal KL-divergence term to regularize the latent

324 space. The use of a latent space rather than raw audio waveforms significantly reduces computational
 325 requirements while preserving perceptual quality. The causal nature of the VAE ensures that both
 326 encoding and decoding operations can be performed in a streaming fashion, making the entire system
 327 suitable for real-time applications where low latency is critical. [The detailed implementation of](#)
 328 [AudioVAE can be found in Appendix D.](#)

329 4 EXPERIMENTS AND RESULTS

330 4.1 EXPERIMENTAL SETUP

331 **Datasets** We conducted experiments on two primary datasets: 1) **Large-scale Bilingual Corpus**:
 332 To explore the best performance, we collected an internal large-scale, bilingual dataset totaling over
 333 1 million hours, mainly comprising of Chinese and English speech. 2) **Emilia Dataset**: For com-
 334 parisons and ablation studies, we used the publicly available Emilia dataset (He et al., 2024) (95K
 335 hours). All audio was resampled to 16kHz mono, processed with source separation, voice activity
 336 detection (VAD), and automatic speech recognition (ASR) system to obtain text-audio alignment.

337 **Implementation Details** We implemented VoxCPM using the Megatron framework, with a 0.5B-
 338 parameter configuration, comprising a 24-layer Text-Semantic Language Model (TSLM), initialized
 339 from the pre-trained MiniCPM-4-0.5B (Team et al., 2025)¹, and a randomly initialized 6-layer
 340 Residual Acoustic Language Model (RALM). We trained two models for comparisons: 1) **VoxCPM**
 341 was trained with internal large-scale bilingual corpus for 500K steps using 40 NVIDIA H100 GPUs;
 342 2) **VoxCPM-Emilia** was trained on the Emilia dataset for 200K steps using 24 H100 GPUs. Both
 343 used the AdamW optimizer with a peak learning rate of 1×10^{-4} and a Warmup-Stable-Decay
 344 (WSD) schedule (Hu et al., 2024). All ablation studies followed the same 200K-step training pro-
 345 tocol on 8 H100 GPUs using the Emilia dataset, employing a fixed learning rate (i.e., without the
 346 WSD schedule) of 1×10^{-4} to ensure a consistent comparison.

347 **Evaluation Metrics and Benchmarks** We employed comprehensive subjective and objective eval-
 348 uations. Objective metrics included Word / Character Error Rate (WER / CER) for intelligibility,
 349 speaker embedding cosine similarity (SIM) for voice cloning, and DNSMOS for overall quality.
 350 Subjective evaluation involved Mean Opinion Score (MOS) tests rated by 20 native speakers on
 351 naturalness (N-MOS) and speaker similarity (S-MOS) using 5-point scales. Models were assessed
 352 on two challenging benchmarks: 1) **SEED-TTS-EVAL**, focusing on general TTS intelligibility and
 353 similarity in English and Chinese, including a “Hard” set with complex sentences; 2) **CV3-EVAL**,
 354 derived from CosyVoice 3 competition, emphasizing expressive and in-the-wild voice cloning.

355 **Baselines** We compared VoxCPM against a wide range of state-of-the-art open-source TTS systems,
 356 including CosyVoice series (Du et al., 2024a;b), MaskGCT (Wang et al., 2025c), F5-TTS (Chen
 357 et al., 2024), SparkTTS (Wang et al., 2025b), FireRedTTS series (Guo et al., 2024; Xie et al., 2025),
 358 IndexTTS 2 (Zhou et al., 2025), HiggsAudio v2 and so on. All baseline results were obtained using
 359 official implementations with default settings, or as reported in their original papers. Details of
 360 compared models see Appendix E.

361 4.2 MAIN RESULTS: COMPARISON WITH STATE-OF-THE-ART TTS

362 As shown in Table 1, VoxCPM achieves state-of-the-art performance among open-source models
 363 on the SEED-TTS-EVAL benchmark. It attains an English WER of 1.85% and a Chinese CER
 364 of 0.93%, surpassing strong competitors like IndexTTS2 and CosyVoice2. Concurrently, VoxCPM
 365 maintains high speaker similarity, with SIM scores of 72.9% (EN) and 77.2% (ZH). This demon-
 366 strates that the proposed semi-discrete bottleneck effectively balances intelligibility and expressivity
 367 by hierarchical semantic-acoustic modeling, mitigating the instability common in continuous mod-
 368 els while preserving details often lost in discrete models. The VoxCPM-Emilia variant, trained on a
 369 smaller public dataset, delivers competitive results (EN-WER: 2.34%, ZH-CER: 1.11%). [When](#)
 370 [compared VoxCPM-Emilia against competitive AR models trained on similar data scales \(e.g.,](#)
 371 [CosyVoice2, SparkTTS, FireRedTTS\), our model consistently outperforms them in stability and](#)
 372 [similarity. While some NAR models like MaskGCT achieve higher objective metrics, AR models](#)
 373 [typically excel in prosodic naturalness and expressiveness in the subjective evaluations \(as shown in](#)

374 ¹<https://huggingface.co/openbmb/Minicpm4-0.5B>

378
379
380 Table 1: Performance on Seed-TTS-eval Benchmark
381
382
383
384
385
386
387
388
389
390
391

Model	Params	Data/hrs	EN		ZH		Hard	
			WER ↓	SIM ↑	CER ↓	SIM ↑	CER ↓	SIM ↑
F5-TTS	0.3B	100K	2.00	67.0	1.53	76.0	8.67	71.3
MaskGCT	1B	100K	2.62	71.7	2.27	77.4	-	-
CosyVoice	0.3B	170K	4.29	60.9	3.63	72.3	11.75	70.9
CosyVoice2	0.5B	170K	3.09	65.9	1.38	75.7	6.83	72.4
SparkTTS	0.5B	100K	3.14	57.3	1.54	66.0	-	-
FireRedTTS	0.5B	248K	3.82	46.0	1.51	63.5	17.45	62.1
FireRedTTS-2	-	1.4M	1.95	66.5	1.14	73.6	-	-
Qwen2.5-Omni	7B	-	2.72	63.2	1.70	75.2	7.97	74.7
OpenAudio-s1-mini	0.5B	2M	1.94	55.0	1.18	68.5	23.37	64.3
IndexTTS 2	1.5B	55K	2.23	70.6	1.03	76.5	7.12	75.5
VibeVoice	1.5B	-	3.04	68.9	1.16	74.4	-	-
HiggsAudio-v2	3B	10M	2.44	67.7	1.50	74.0	55.07	65.6
VoxCPM-Emilia	0.5B	100K	2.34	68.1	1.11	74.0	12.46	69.8
VoxCPM	0.5B	1.8M	1.85	72.9	0.93	77.2	8.87	73.0

392
393
394 Table 2: Performance on CV3-eval Benchmark. *denotes close-sourced systems.
395

Model	CV3-EVAL		CV3-Hard-ZH			CV3-Hard-EN		
	ZH-CER ↓	EN-WER ↓	CER ↓	SIM ↑	DNSMOS↑	WER ↓	SIM ↑	DNSMOS↑
F5-TTS	5.47	8.90	-	-	-	-	-	-
SparkTTS	5.15	11.0	-	-	-	-	-	-
GPT-Sovits	7.34	12.5	-	-	-	-	-	-
CosyVoice2	4.08	6.32	12.58	72.6	3.81	11.96	66.7	3.95
OpenAudio-s1-mini	4.00	5.54	18.1	58.2	3.77	12.4	55.7	3.89
IndexTTS2	3.58	4.45	12.8	74.6	3.65	8.78	74.5	3.80
HiggsAudio-v2	9.54	7.89	41.0	60.2	3.39	10.3	61.8	3.68
CosyVoice3-0.5B*	3.89	5.24	14.15	78.6	3.75	9.04	75.9	3.92
CosyVoice3-1.5B*	3.91	4.99	9.77	78.5	3.79	10.55	76.1	3.95
VoxCPM-Emilia	4.47	5.23	22.2	62.6	3.47	10.00	62.6	3.68
VoxCPM	3.40	4.04	12.9	66.1	3.59	7.89	64.3	3.74

406
407
408
409 Table 3). This highlights the data efficiency and architectural robustness of our approach, as the
410 FSQ bottleneck stabilizes the learning of semantic-acoustic representations even with less training
411 data. Notably, while DiTAR’s phoneme-based approach shows slightly better stability, VoxCPM’s
412 use of BPE tokens with pre-trained LLM initialization provides superior text understanding capa-
413 bilities and eliminates dependency on external phonemizers. Besides, our hierarchical design with
414 residual acoustic modeling reduces the fundamental limitation of direct continuous token modeling,
415 as evidenced in ablation studies.416 On the CV3-EVAL benchmark (Table 2), designed to evaluate expressive and in-the-wild perfor-
417 mance, VoxCPM excels with a ZH-CER of 3.40% and an EN-WER of 4.04%. Its robustness is
418 further confirmed on the challenging CV3 Hard-Test set, where it achieves an EN-WER of 7.89%,
419 outperforming even close-sourced CosyVoice 3. However, VoxCPM achieves a relatively lower
420 DNSMOS score compared to others, as the prompt audios used in CV3-Hard inherently have a low
421 DNSMOS (around 3.5), which demonstrates its faithful cloning of the recording environment and
422 *vibe*. These results underscore the model’s capability to handle complex, realistic inputs, a strength
423 attributed to the RALM’s role in recovering fine-grained acoustic details subsequent to the TSLM-
424 FSQ-based semantic-prosodic modeling.425 Subjective evaluations (Table 3) further validate the objective findings, with VoxCPM achieving
426 competitive performance across both languages. On English tests, VoxCPM obtains the highest
427 scores in speaker similarity and good results in naturalness. For Chinese, while VoxCPM trails In-
428 dexTTS 2 in naturalness, it achieves slightly superior speaker similarity. We found that many prompt
429 audios from the Seed-TTS-Eval test set contain disfluencies or exhibit a monotonous tone, which
430 inherently constrains the naturalness of our cloned outputs. This pattern suggests that VoxCPM ex-
431 ceels at voice cloning consistency, while IndexTTS 2 may have advantages in prosodic naturalness
432 for Chinese. VoxCPM-Emilia shows competitive speaker similarity but relatively lower naturalness,
433 highlighting the impact of training data scale.

Table 3: Subjective Evaluations in terms of Naturalness and Speaker Similarity. **Note:** We select the competitive baseline models for subjective comparison based on objective results.

Model	ZH		EN	
	N-MOS	S-MOS	N-MOS	S-MOS
MaskGCT	3.20 \pm 0.11	3.77 \pm 0.11	3.84 \pm 0.11	4.00 \pm 0.10
CosyVoice 2	3.38 \pm 0.12	4.01 \pm 0.10	4.14 \pm 0.09	3.97 \pm 0.10
IndexTTS 2	4.25 \pm 0.09	4.05 \pm 0.09	4.03 \pm 0.10	4.16 \pm 0.09
VoxCPM-Emilia	3.79 \pm 0.12	3.99 \pm 0.11	3.91 \pm 0.10	4.10 \pm 0.09
VoxCPM	4.10 \pm 0.10	4.11 \pm 0.10	4.11 \pm 0.09	4.18 \pm 0.09

4.3 ABLATION STUDY: EFFECT OF THE SEMI-DISCRETE BOTTLENECK

As shown in Table 4, the ablation studies on the FSQ bottleneck dimensionality (More details can be found in Appendix Table 9) provide critical insights. The catastrophic performance degradation of the purely continuous model (w/o FSQ), especially on hard cases (ZH-CER: 24.92%), validates our core hypothesis: entangling semantic planning and acoustic rendering in a continuous space leads to instability. Without the inductive bias imposed by FSQ, the model struggles to separate these tasks, resulting in error accumulation on complex utterances.

The optimal performance observed at FSQ levels (FSQ-d128/d256) reveals a key trade-off. Lower dimensions (e.g., FSQ-d4) over-constrain the representation, limiting prosodic capacity. Higher dimensions (e.g., FSQ-d1024) provide insufficient discretization strength, allowing task entanglement to persist. The peak at FSQ-d256 indicates the bottleneck creates an effective “summary space”: discrete enough to stabilize long-range semantic planning yet continuous enough to retain crucial prosodic and speaker information, thereby enforcing a beneficial division of labor within the model.

4.4 ABLATION STUDY: EFFECT OF RESIDUAL ACOUSTIC MODELING

As shown in Table 4, the ablation studies about the residual language modeling validate our core architectural innovations. Notably, the purely continuous variant (w/o RALM: TSLM \rightarrow LocDiT)—analogous to DiTAR’s approach—shows significantly degraded performance, particularly on challenging cases. The performance gap persists across different TSLM configurations, confirming that the challenge is fundamental to the learning objective rather than parameter allocation. This conclusively demonstrates the advantage of our explicit separation between semantic and acoustic modeling. To isolate the benefits of our hierarchical architecture from simple capacity effects, we compared single-stream models with identical initialization foundation but varying depths: [w/o RALM: TSLM(24 layers, LM init.)] vs. [w/o RALM: TSLM(30 layers, partial LM init.)]. The gains from increasing capacity is marginal (e.g., EN-WER from 4.34 to 4.12), while the gains from introducing hierarchical structure is larger in default setting (e.g., EN-WER 2.98). This confirms that the hierarchical TSLM/RALM separation is the dominant factor for stability and expressiveness, significantly outweighing the benefit of merely increased capacity. Furthermore, the hierarchical design exhibits superior performance compared to its single-stream counterpart, even under fully random initialization ([Hierarchical, w/o LM init. in TSLM] vs. [w/o RALM: TSLM(30 layers, random init.)]). This simultaneous improvement demonstrates that the hierarchical residual design provides intrinsic benefit for a specialized division of labor, which is effective even without the strong semantic grounding from pre-trained parameters.

Secondly, the critical role of residual acoustic input is further evidenced by the substantial degradation when ablating original acoustic embeddings (w/o $E_{<i}$ in RALM), highlighting that the RALM requires fine-grained acoustic information to accurately recover acoustic details. Finally, the best performance of the default setting demonstrates the effectiveness of the residual connection. By summing the TSLM and RALM hidden states, the model explicitly delegates semantic-prosodic planning to the TSLM and acoustic refinement to the RALM, achieving optimal integration.

Finally, the effect of pre-training initialization is intuitive: removing pre-trained text LM initialization results in a significant degradation in intelligibility (e.g., EN-WER 2.98 vs. 5.24). This confirms that the pre-trained knowledge is critical for establishing the TSLM’s initial capability and stability. We observe that models trained from random initialization shows a marginal increase in SIM.

486 suggesting that without the strong linguistic guidance from the pre-trained LLM, the model might
 487 implicitly allocate more capacity to acoustic feature modeling.
 488

489 Table 4: Ablation Studies about FSQ bottleneck dimensions and core architecture designs.
 490

491 Model Setting	492 EN		493 ZH		494 ZH-hard case	
	495 WER ↓	496 SIM ↑	497 CER ↓	498 SIM ↑	499 CER ↓	500 SIM ↑
501 default setting (w/ FSQ: d256s9)	502 2.98	503 62.6	504 1.77	505 70.4	506 18.19	507 64.9
508 w/ FSQ: d4s9	509 5.18	510 59.3	511 4.05	512 68.0	513 19.55	514 62.3
515 w/ FSQ: d128s9	516 3.43	517 62.2	518 1.67	519 70.7	520 16.76	521 65.7
523 w/ FSQ: d1024s9	524 3.07	525 62.0	526 2.38	527 69.8	528 20.38	529 64.7
532 w/o FSQ: d1024s∞	533 3.67	534 62.1	535 2.30	536 69.6	537 24.92	538 63.5
541 Hierarchical, w/o LM init. in TSLM	542 5.24	543 63.4	544 2.41	545 70.9	546 24.66	547 65.6
549 w/o RALM: TSLM (24 layers, LM init.) → LocDiT	550 4.34	551 61.8	552 3.05	553 69.4	554 25.00	555 63.8
558 w/o RALM: TSLM (30 layers, random init.) → LocDiT	559 5.35	560 62.6	561 3.46	562 69.8	563 30.40	564 63.9
567 w/o RALM: TSLM (30 layers, partial LM init.) → LocDiT	568 4.12	569 62.0	570 3.07	571 69.6	572 26.20	573 63.1
577 w/o $E_{<i}$ in RALM: TSLM → ALM → LocDiT	578 4.91	579 60.9	580 4.94	581 68.1	582 27.17	583 61.7
587 w/o h_{residual} in condition: TSLM → FSQ → LocDiT	588 3.86	589 58.3	590 3.05	591 67.6	592 23.65	593 61.7

501
4.5 ANALYSIS AND DISCUSSION

502
503 **Analysis of Hierarchical Representations** T-SNE visualizations (Appendix Figure 2 to 5) confirm
 504 the specialized roles of TSLM and RALM. TSLM-FSQ outputs form semantic-prosodic structures
 505 closely tied to text content, whereas RALM residuals exhibit strong speaker-related variations for
 506 acoustic rendering. This functional specialization validates the efficacy of our hierarchical residual
 507 modeling. More details and analysis can be found in Appendix F.5.

508 **Expressive Synthesis Capabilities** Beyond quantitative metrics and visualizations, VoxCPM shows
 509 good expressive synthesis capabilities directly from text benefiting from the architecture design and
 510 training data. When not using prompt speech, the model tends to express suitable style from con-
 511 textual cues, also shown in F.5. We strongly recommend readers to listen our demo samples.

512 **Scalability and Efficiency** The performance improvement from VoxCPM-Emilia to VoxCPM high-
 513 lights the architecture’s scalability with increased data. The hierarchical design allows larger models
 514 to effectively utilize increased capacity for learning complex patterns. In terms of inference effi-
 515 ciency, VoxCPM-0.5B achieves a real-time factor (RTF) of 0.17 on a single NVIDIA RTX 4090,
 516 confirming practical deployment feasibility.

518
519 5 CONCLUSION

520
521 In this work, we resolve the fundamental trade-off between expressivity and stability in text-to-
 522 speech synthesis by introducing a unified, end-to-end framework based on hierarchical semantic-
 523 acoustic modeling with semi-discrete residual representations. Our approach leverages a differenti-
 524 able quantization bottleneck to induce a natural separation of concerns: a text-semantic language
 525 model captures high-level semantic-prosodic structure, while a residual acoustic model recovers
 526 fine-grained details. This eliminates the dependency on external discrete speech tokenizers and mit-
 527 igates the error accumulation that plagues purely continuous autoregressive models. Extensive ex-
 528 periments demonstrate that our model achieves state-of-the-art zero-shot TTS performance among
 529 open-source systems, excelling in both intelligibility and speaker similarity. The success of Vox-
 530 CPM validates that learning structured, regularized latent spaces provides a principled foundation
 531 for expressive generative audio modeling.

532
533 REFERENCES

534 Keyu An, Zhiyu Zhang, Changfeng Gao, Yabin Li, Zhendong Peng, Haoxu Wang, Zhihao Du, Han
 535 Zhao, Zhifu Gao, and Xiangang Li. Mela-tts: Joint transformer-diffusion model with representa-
 536 tion alignment for speech synthesis. *arXiv preprint arXiv:2509.14784*, 2025.

537 Matthew Baas, Pieter Scholtz, Arnav Mehta, Elliott Dyson, Akshat Prakash, and Herman Kamper.
 538 Mars6: A small and robust hierarchical-codec text-to-speech model. In *ICASSP 2025-2025 IEEE*
 539 *International Conference on Acoustics, Speech and Signal Processing (ICASSP)*, pp. 1–5. IEEE,
 2025.

540 Zalán Borsos, Raphaël Marinier, Damien Vincent, Eugene Kharitonov, Olivier Pietquin, Matt Shar-
 541 ifi, Dominik Roblek, Olivier Teboul, David Grangier, Marco Tagliasacchi, et al. Audiolfm: a
 542 language modeling approach to audio generation. *IEEE/ACM transactions on audio, speech, and*
 543 *language processing*, 31:2523–2533, 2023a.

544 Zalán Borsos, Matt Sharifi, Damien Vincent, Eugene Kharitonov, Neil Zeghidour, and Marco
 545 Tagliasacchi. Soundstorm: Efficient parallel audio generation. *arXiv preprint arXiv:2305.09636*,
 546 2023b.

548 Edresson Casanova, Kelly Davis, Eren Gölge, Görkem Göknar, Iulian Gulea, Logan Hart, Aya Al-
 549 jafari, Joshua Meyer, Reuben Morais, Samuel Olayemi, et al. Xtts: a massively multilingual
 550 zero-shot text-to-speech model. *arXiv preprint arXiv:2406.04904*, 2024.

551 Sanyuan Chen, Chengyi Wang, Yu Wu, Ziqiang Zhang, Long Zhou, Shujie Liu, Zhuo Chen, Yanqing
 552 Liu, Huaming Wang, Jinyu Li, et al. Neural codec language models are zero-shot text to speech
 553 synthesizers. *IEEE Transactions on Audio, Speech and Language Processing*, 2025.

555 Yushen Chen, Zhikang Niu, Ziyang Ma, Keqi Deng, Chunhui Wang, Jian Zhao, Kai Yu, and Xie
 556 Chen. F5-tts: A fairytaler that fakes fluent and faithful speech with flow matching. *CoRR*, 2024.

557 Alexandre Défossez, Jade Copet, Gabriel Synnaeve, and Yossi Adi. High fidelity neural audio
 558 compression. *arXiv preprint arXiv:2210.13438*, 2022.

560 Wei Deng, Siyi Zhou, Jingchen Shu, Jinchao Wang, and Lu Wang. Indextts: An industrial-level con-
 561 trollable and efficient zero-shot text-to-speech system. *arXiv preprint arXiv:2502.05512*, 2025.

562 Zhihao Du, Qian Chen, Shiliang Zhang, Kai Hu, Heng Lu, Yexin Yang, Hangrui Hu, Siqi Zheng, Yue
 563 Gu, Ziyang Ma, et al. Cosyvoice: A scalable multilingual zero-shot text-to-speech synthesizer
 564 based on supervised semantic tokens. *arXiv preprint arXiv:2407.05407*, 2024a.

566 Zhihao Du, Yuxuan Wang, Qian Chen, Xian Shi, Xiang Lv, Tianyu Zhao, Zhifu Gao, Yexin Yang,
 567 Changfeng Gao, Hui Wang, et al. Cosyvoice 2: Scalable streaming speech synthesis with large
 568 language models. *arXiv preprint arXiv:2412.10117*, 2024b.

569 Zhihao Du, Changfeng Gao, Yuxuan Wang, Fan Yu, Tianyu Zhao, Hao Wang, Xiang Lv, Hui Wang,
 570 Chongjia Ni, Xian Shi, et al. Cosyvoice 3: Towards in-the-wild speech generation via scaling-up
 571 and post-training. *arXiv preprint arXiv:2505.17589*, 2025.

573 Hao-Han Guo, Yao Hu, Kun Liu, Fei-Yu Shen, Xu Tang, Yi-Chen Wu, Feng-Long Xie, Kun Xie,
 574 and Kai-Tuo Xu. Fireredtts: A foundation text-to-speech framework for industry-level generative
 575 speech applications. *arXiv preprint arXiv:2409.03283*, 2024.

576 Yichen Han, Xiaoyang Hao, Keming Chen, Weibo Xiong, Jun He, Ruonan Zhang, Junjie Cao, Yue
 577 Liu, Bowen Li, Dongrui Zhang, et al. Quantize more, lose less: Autoregressive generation from
 578 residually quantized speech representations. *arXiv preprint arXiv:2507.12197*, 2025.

580 Haorui He, Zengqiang Shang, Chaoren Wang, Xuyuan Li, Yicheng Gu, Hua Hua, Liwei Liu, Chen
 581 Yang, Jiaqi Li, Peiyang Shi, et al. Emilia: An extensive, multilingual, and diverse speech dataset
 582 for large-scale speech generation. In *2024 IEEE Spoken Language Technology Workshop (SLT)*,
 583 pp. 885–890. IEEE, 2024.

584 Shengding Hu, Yuge Tu, Xu Han, Chaoqun He, Ganqu Cui, Xiang Long, Zhi Zheng, Yewei Fang,
 585 Yuxiang Huang, Weilin Zhao, et al. Minicpm: Unveiling the potential of small language models
 586 with scalable training strategies. *arXiv preprint arXiv:2404.06395*, 2024.

587 Dongya Jia, Zhuo Chen, Jiawei Chen, Chenpeng Du, Jian Wu, Jian Cong, Xiaobin Zhuang, Chumin
 588 Li, Zhen Wei, Yuping Wang, et al. Ditar: Diffusion transformer autoregressive modeling for
 589 speech generation. *arXiv preprint arXiv:2502.03930*, 2025.

591 Eugene Kharitonov, Damien Vincent, Zalán Borsos, Raphaël Marinier, Sertan Girgin, Olivier
 592 Pietquin, Matt Sharifi, Marco Tagliasacchi, and Neil Zeghidour. Speak, read and prompt: High-
 593 fidelity text-to-speech with minimal supervision. *Transactions of the Association for Computa-
 tional Linguistics*, 11:1703–1718, 2023.

594 Rithesh Kumar, Prem Seetharaman, Alejandro Luebs, Ishaan Kumar, and Kundan Kumar. High-
 595 fidelity audio compression with improved rvqgan. *Advances in Neural Information Processing*
 596 *Systems*, 36:27980–27993, 2023.

597

598 Matthew Le, Apoorv Vyas, Bowen Shi, Brian Karrer, Leda Sari, Rashel Moritz, Mary Williamson,
 599 Vimal Manohar, Yossi Adi, Jay Mahadeokar, et al. Voicebox: Text-guided multilingual universal
 600 speech generation at scale. *Advances in neural information processing systems*, 36:14005–14034,
 601 2023.

602 Sang-Hoon Lee, Ha-Yeong Choi, Seung-Bin Kim, and Seong-Whan Lee. Hierspeech++: Bridg-
 603 ing the gap between semantic and acoustic representation of speech by hierarchical variational
 604 inference for zero-shot speech synthesis. *IEEE Transactions on Neural Networks and Learning*
 605 *Systems*, 2025.

606

607 Naihan Li, Shujie Liu, Yanqing Liu, Sheng Zhao, and Ming Liu. Neural speech synthesis with
 608 transformer network. In *Proceedings of the AAAI conference on artificial intelligence*, volume 33,
 609 pp. 6706–6713, 2019.

610 Tianhong Li, Yonglong Tian, He Li, Mingyang Deng, and Kaiming He. Autoregressive image
 611 generation without vector quantization. *Advances in Neural Information Processing Systems*, 37:
 612 56424–56445, 2024.

613

614 Jiaxuan Liu, Zhaoci Liu, Yajun Hu, Yingying Gao, Shilei Zhang, and Zhenhua Ling. Diffstyletts:
 615 Diffusion-based hierarchical prosody modeling for text-to-speech with diverse and controllable
 616 styles. *arXiv preprint arXiv:2412.03388*, 2024.

617

618 Lingwei Meng, Long Zhou, Shujie Liu, Sanyuan Chen, Bing Han, Shujie Hu, Yanqing Liu, Jinyu
 619 Li, Sheng Zhao, Xixin Wu, et al. Autoregressive speech synthesis without vector quantization.
 620 *arXiv preprint arXiv:2407.08551*, 2024.

621

622 Fabian Mentzer, David Minnen, Eirikur Agustsson, and Michael Tschannen. Finite scalar quantiza-
 623 tion: Vq-vae made simple. In *The Twelfth International Conference on Learning Representations*,
 624 2024.

625

626 Yuto Nishimura, Takumi Hirose, Masanari Ohi, Hideki Nakayama, and Nakamasa Inoue. Hall-e:
 627 Hierarchical neural codec language model for minute-long zero-shot text-to-speech synthesis. In
 628 *The Thirteenth International Conference on Learning Representations*, 2025.

629

630 Marco Pasini, Javier Nistal, Stefan Lattner, and George Fazekas. Continuous autoregressive models
 631 with noise augmentation avoid error accumulation. *arXiv preprint arXiv:2411.18447*, 2024.

632

633 Puyuan Peng, Po-Yao Huang, Shang-Wen Li, Abdelrahman Mohamed, and David Harwath. Voice-
 634 craft: Zero-shot speech editing and text-to-speech in the wild. In *Proceedings of the 62nd Annual*
 635 *Meeting of the Association for Computational Linguistics (Volume 1: Long Papers)*, pp. 12442–
 636 12462, 2024.

637

638 Zhiliang Peng, Jianwei Yu, Wenhui Wang, Yaoyao Chang, Yutao Sun, Li Dong, Yi Zhu, Wei-
 639 jiang Xu, Hangbo Bao, Zehua Wang, et al. Vibevoice technical report. *arXiv preprint*
 640 *arXiv:2508.19205*, 2025.

641

642 Wei Ping, Kainan Peng, Andrew Gibiansky, Sercan O Arik, Ajay Kannan, Sharan Narang, Jonathan
 643 Raiman, and John Miller. Deep voice 3: Scaling text-to-speech with convolutional sequence
 644 learning. *arXiv preprint arXiv:1710.07654*, 2017.

645

646 Yi Ren, Chenxu Hu, Xu Tan, Tao Qin, Sheng Zhao, Zhou Zhao, and Tie-Yan Liu. Fastspeech
 647 2: Fast and high-quality end-to-end text to speech. In *International Conference on Learning*
 648 *Representations*, 2020.

649

650 Jonathan Shen, Ruoming Pang, Ron J Weiss, Mike Schuster, Navdeep Jaitly, Zongheng Yang,
 651 Zhifeng Chen, Yu Zhang, Yuxuan Wang, Rj Skerry-Ryan, et al. Natural tts synthesis by con-
 652 ditioning wavenet on mel spectrogram predictions. In *2018 IEEE international conference on*
 653 *acoustics, speech and signal processing (ICASSP)*, pp. 4779–4783. IEEE, 2018.

648 Kai Shen, Zeqian Ju, Xu Tan, Eric Liu, Yichong Leng, Lei He, Tao Qin, Jiang Bian, et al. Natural-
 649 speech 2: Latent diffusion models are natural and zero-shot speech and singing synthesizers. In
 650 *The Twelfth International Conference on Learning Representations*, 2023.

651

652 MiniCPM Team, Chaojun Xiao, Yuxuan Li, Xu Han, Yuzhuo Bai, Jie Cai, Haotian Chen, Wentong
 653 Chen, Xin Cong, Ganqu Cui, et al. Minicpm4: Ultra-efficient llms on end devices. *arXiv preprint*
 654 *arXiv:2506.07900*, 2025.

655 Chunhui Wang, Chang Zeng, Bowen Zhang, Ziyang Ma, Yefan Zhu, Zifeng Cai, Jian Zhao,
 656 Zhonglin Jiang, and Yong Chen. Ham-tts: Hierarchical acoustic modeling for token-based zero-
 657 shot text-to-speech with model and data scaling. *arXiv preprint arXiv:2403.05989*, 2024.

658

659 Hui Wang, Shujie Liu, Lingwei Meng, Jinyu Li, Yifan Yang, Shiwan Zhao, Haiyang Sun, Yanqing
 660 Liu, Haoqin Sun, Jiaming Zhou, et al. Felle: Autoregressive speech synthesis with token-wise
 661 coarse-to-fine flow matching. *arXiv preprint arXiv:2502.11128*, 2025a.

662

663 Xinsheng Wang, Mingqi Jiang, Ziyang Ma, Ziyu Zhang, Songxiang Liu, Linqin Li, Zheng Liang,
 664 Qixi Zheng, Rui Wang, Xiaoqin Feng, et al. Spark-tts: An efficient llm-based text-to-speech
 665 model with single-stream decoupled speech tokens. *arXiv preprint arXiv:2503.01710*, 2025b.

666

667 Yuancheng Wang, Haoyue Zhan, Liwei Liu, Ruihong Zeng, Haotian Guo, Jiachen Zheng, Qiang
 668 Zhang, Xueyao Zhang, Shunsi Zhang, and Zhizheng Wu. Maskgct: Zero-shot text-to-speech with
 669 masked generative codec transformer. In *The Thirteenth International Conference on Learning
 670 Representations*, 2025c.

671

672 Chun Yat Wu, Jiajun Deng, Guinan Li, Qiuqiang Kong, and Simon Lui. Clear: Continuous la-
 673 tent autoregressive modeling for high-quality and low-latency speech synthesis. *arXiv preprint*
 674 *arXiv:2508.19098*, 2025.

675

676 Kun Xie, Feiyu Shen, Junjie Li, Fenglong Xie, Xu Tang, and Yao Hu. Fireredtts-2: Towards
 677 long conversational speech generation for podcast and chatbot. *arXiv preprint arXiv:2509.02020*,
 678 2025.

679

680 Shu-wen Yang, Po-Han Chi, Yung-Sung Chuang, Cheng-I Jeff Lai, Kushal Lakhota, Yist Y Lin,
 681 Andy T Liu, Jiatong Shi, Xuankai Chang, Guan-Ting Lin, et al. Superb: Speech processing
 682 universal performance benchmark. *Interspeech 2021*, 2021.

683

684 Siyi Zhou, Yiquan Zhou, Yi He, Xun Zhou, Jinchao Wang, Wei Deng, and Jingchen Shu. Indextts2:
 685 A breakthrough in emotionally expressive and duration-controlled auto-regressive zero-shot text-
 686 to-speech. *arXiv preprint arXiv:2506.21619*, 2025.

687

688 Xinfa Zhu, Wenjie Tian, and Lei Xie. Autoregressive speech synthesis with next-distribution pre-
 689 diction. *arXiv preprint arXiv:2412.16846*, 2024.

690

691

692

693

694

695

696

697

698

699

700

701

702 **A THE USE OF LARGE LANGUAGE MODELS (LLMs)**
703704
705 In accordance with ICLR policy, we disclose that a large language model (LLM), specifically
706 Gemini-2.5 and DeepSeek, was used as a general-purpose assistive tool during the writing of this
707 paper. The LLM was employed solely for the purpose of text polishing and refinement, specifically
708 to assist with improving grammar, enhancing word choice, and increasing the overall readability
709 and fluency of the manuscript. However, the model played no role in the intellectual or scientific
710 contributions of this work, including research ideation, experimental design, result analysis, or con-
711 clusion drawing. All such core content is solely the product of the human authors, who take full
712 responsibility for the research presented.
713714 **B REPRODUCIBILITY STATEMENT**
715716 Inference codes are available at codes.zip. Training was conducted using the Megatron framework
717 on 40 NVIDIA H100 GPUs for the main VoxCPM model and 24 H100 GPUs for VoxCPM-Emilia.
718 Ablation studies used 8 H100 GPUs. Full details about hyperparameters are in Section D.
719720 **C ETHICS STATEMENT**
721722 Since our zero-shot TTS model achieves high-quality speech synthesis with the ability to closely
723 mimic speaker characteristics, it carries potential risks of misuse. These risks include, but are
724 not limited to, spoofing voice authentication systems or impersonating a specific speaker without
725 their consent. Our experiments were conducted under the assumption that the use of any reference
726 speaker’s voice is authorized and intended for legitimate synthesis purposes. To mitigate these risks,
727 we strongly advocate for the development of robust synthesized speech detection algorithms. Fur-
728 thermore, we believe it is crucial to establish clear ethical guidelines and reporting mechanisms for
729 the responsible deployment of such technology.
730731
732 **D IMPLEMENTATION DETAILS OF VOXCPM**
733734 **D.1 MODEL ARCHITECTURE**
735736 VoxCPM consists of a 24-layer TSLM (initialized from MiniCPM-4-0.5B) and a 6-layer RALM.
737 The FSQ layer uses 256 dimensions with 9 scalar levels. The diffusion decoder has 4 layers, opti-
738 mized for high-efficacy latent generation, as shown in Table 5
739740 For Audio VAE, it operates at a 25 Hz frame rate, designed to be compatible with the streaming
741 nature of VoxCPM. The VAE’s architecture is inspired by DAC, with both its encoder and decoder
742 implemented using stacked Causal Convolutional Networks (Causal CNNs). For 16 kHz single-
743 channel audio, the encoder achieves a 640x downsampling factor through a series of strided convolu-
744 tions with a stride sequence of [2, 5, 8, 8], compressing the audio into a 25 Hz latent representation.
745 The decoder then reconstructs the original waveform by upsampling from this latent representation.
746 The training objectives consist of an adversarial (GAN) loss, a Mel-spectrogram loss, and a KL
747 divergence loss, with the latter’s weight set to 5e-5.
748749 **D.2 TRAINING CONFIGURATION**
750751 Both VoxCPM and VoxCPM-Emilia employed the Warmup-Stable-Decay (WSD) training strategy,
752 which we found essential for optimal convergence. Specifically, the decay phase with annealing
753 to a very low learning rate (combined with batch size doubling) significantly enhances model per-
754 formance, particularly for zero-shot speaker similarity, as demonstrated in Table 10. All ablation
755 studies followed the same 200K-step training protocol on 8 H100 GPUs using the Emilia dataset,
employing a fixed learning rate of 1×10^{-4} to ensure consistent comparisons.

756 Table 5: The model architecture and parameters of VoxCPM-0.5B.
757

758 Module	759 Configuration	760 Parameters
760 LocEnc	761 4 layers, 1024 hidden dim, 4096 FFN dim	762 59M
761 TSLM	762 24 layers, 1024 hidden dim, 4096 FFN dim	763 433M
762 FSQ	763 256 dimensions, 9 quantization levels	764 0.5M
763 RALM	764 6 layers, 1024 hidden dim, 4096 FFN dim	765 89M
764 LocDiT	765 4 layers, 1024 hidden dim, 4096 FFN dim	766 64M
765 Stop Predictor	766 3-layer MLP, 1024 hidden dim, 2 output dim	767 1M
766 patch-size	767 2 (that is, TSLM and RALM work in 12.5Hz token rate)	768 -
767 AudioVAE	768 16kHz waveform \rightarrow 25Hz latents (downsampling at [2, 5, 8, 8])	769 75M

768 Table 6: Training configurations for VoxCPM variants.
769

770 Model	771 Phase	772 Learning Rate	773 Tokens/Batch	774 Steps	775 GPUs
772 VoxCPM	773 Stable	774 1×10^{-4}	775 4,096	776 400K	777 $40 \times \text{H100}$
773 VoxCPM	774 Decay	775 $1 \times 10^{-4} \rightarrow 5 \times 10^{-6}$	776 8,192	777 100K	778 $40 \times \text{H100}$
774 VoxCPM-Emilia	775 Stable	776 1×10^{-4}	777 4,096	778 150K	779 $24 \times \text{H100}$
775 VoxCPM-Emilia	776 Decay	777 $1 \times 10^{-4} \rightarrow 5 \times 10^{-6}$	778 8,192	779 50K	780 $24 \times \text{H100}$
776 VoxCPM-ablation	777 Stable	778 1×10^{-4}	779 4,096	780 200K	781 $8 \times \text{H100}$

781

E DETAILS OF BASELINES

782 We compared VoxCPM against several state-of-the-art TTS systems, focusing on open-source mod-
783 els from the SEED-TTS-EVAL and CV3-EVAL benchmarks. Below, we describe the key baselines,
784 their architectures, training data, and how evaluation samples were generated.

- 785 • **CosyVoice Series** (Du et al., 2024a;b; 2025): A family of TTS models leveraging su-
786 pervised semantic tokens and multi-stage pipelines. CosyVoice (Du et al., 2024a) uses a
787 transformer-based architecture with S3Tokenizer, trained on approximately 170K hours
788 of multilingual speech data (primarily English and Chinese). CosyVoice2 (Du et al.,
789 2024b) enhances this with text-based LLM initialization, and introduces streaming syn-
790 thesis for low-latency synthesis. CosyVoice3 (Du et al., 2025) further leverages in-the-
791 wild speech data, and proposes a novel speech tokenizer to capture prosody, with pow-
792 erful post-training techniques. We used officially released checkpoints from <https://github.com/FunAudioLLM/CosyVoice> with default settings to generate sam-
793 ples.
- 794 • **MaskGCT** (Wang et al., 2025c): A non-autoregressive transformer model that employs
795 masked generative transformers to predict discrete speech tokens derived from a neural
796 audio codec and SSL tokens. It is trained on the Emilia dataset and achieves a strong
797 performance on zero-shot TTS. Besides, it can control the duration precisely. Samples
798 were generated using the official implementation provided at <https://github.com/open-mmlab/Amphion/tree/main/models/tts/maskgct>.
- 800 • **F5-TTS** (Chen et al., 2024): A non-autoregressive model utilizing flow-matching for effi-
801 cient speech synthesis. It operates on continuous mel-spectrogram representations, also
802 trained on Emilia dataset. We used the official codes and checkpoint from <https://github.com/SWivid/F5-TTS> to generate evaluation samples.
- 803 • **SparkTTS** (Wang et al., 2025b): A language model-based model using single-stream de-
804 coupled speech tokens to improve modeling efficiency. It is trained on 100K hours of
805 bilingual (English and Chinese) dataset VoxBox, enabling it capability to achieve con-
806 trollable speech synthesis. Samples were generated using the official implementation at
807 <https://github.com/SparkAudio/Spark-TTS>.
- 808 • **FireRedTTS Series** (Guo et al., 2024; Xie et al., 2025): FireRedTTS presents a founda-
809 tion TTS framework for industry-level generative speech application. FireRedTTS2 fur-

810
 811
 812
 813
 814
 815
 816
 817
 818
 819
 820
 821
 822
 823
 824
 825
 826
 827
 828
 829
 830
 831
 832
 833
 834
 835
 836
 837
 838
 839
 840
 841
 842
 843
 844
 845
 846
 847
 848
 849
 850
 851
 852
 853
 854
 855
 856
 857
 858
 859
 860
 861
 862
 863
 ther employs it for long-form multi-speaker dialogue. FireRedTTS-2 improves scalability with a refined transformer architecture, trained on 1.1M hours of monologue speech data and 300k hours of multi-speaker dialogue data. We used official checkpoints from <https://github.com/FireRedTeam/FireRedTTS> for sample generation.

- **IndexTTS2** (Zhou et al., 2025): An autoregressive large-scale TTS model with precise duration control. It also achieves disentanglement between emotional expression and speaker identity, enabling independent control over timbre and emotion. Samples were generated using the official checkpoint from <https://github.com/index-tts/index-tts>.
- **Higgs Audio v2**: A powerful audio foundation model pretrained on over 10 million hours of audio data and a diverse set of text data. It proposes a unified audio tokenizer captures both semantic and acoustic features. We used the official implementation at <https://github.com/boson-ai/higgs-audio> to generate samples.
- **VibeVoice** (Peng et al., 2025): A novel framework designed for generating expressive, long-form, multi-speaker conversational audio, such as podcasts, from text. It presents a continuous speech tokenizers (Acoustic and Semantic) operating at an ultra-low frame rate of 7.5 Hz. Because now the codes are unavailable at <https://github.com/microsoft/VibeVoice>, we use the official results reported in the paper.
- **OpenAudio-s1-mini**: A compact and powerful TTS model (0.5B parameters) using dual-AR architecture and online Reinforcement Learning from Human Feedback (RLHF). Samples were generated using the official implementation at <https://github.com/fishaudio/fish-speech>.

F ADDITIONAL EXPERIMENTAL RESULTS

F.1 COMPREHENSIVE COMPARISONS ON SEED-TTS-EVAL BENCHMARK

In this section, we present comprehensive comparisons covering both open-source and close-source TTS systems. As shown in Table 7, VoxCPM not only outperforms all open-source competitors but also achieves results comparable to several proprietary systems, despite their significantly larger parameter counts and training data scales.

Table 7: Performance on Seed-TTS-eval Benchmark, including close-sourced systems

Model	Params	Open-Source	EN		ZH		Hard	
			WER ↓	SIM ↑	CER ↓	SIM ↑	CER ↓	SIM ↑
MegaTTS3	0.5B	✗	2.79	77.1	1.52	79.0	-	-
DiTAR	0.6B	✗	1.69	73.5	1.02	75.3	-	-
CosyVoice3	0.5B	✗	2.02	71.8	1.16	78.0	6.08	75.8
CosyVoice3	1.5B	✗	2.22	72.0	1.12	78.1	5.83	75.8
Seed-TTS	-	✗	2.25	76.2	1.12	79.6	7.59	77.6
MiniMax-Speech-02	-	✗	1.65	69.2	0.83	78.3	-	-
F5-TTS	0.3B	✓	2.00	67.0	1.53	76.0	8.67	71.3
MaskGCT	1B	✓	2.62	71.7	2.27	77.4	-	-
CosyVoice	0.3B	✓	4.29	60.9	3.63	72.3	11.75	70.9
CosyVoice2	0.5B	✓	3.09	65.9	1.38	75.7	6.83	72.4
SparkTTS	0.5B	✓	3.14	57.3	1.54	66.0	-	-
FireRedTTS	0.5B	✓	3.82	46.0	1.51	63.5	17.45	62.1
FireRedTTS-2		✓	1.95	66.5	1.14	73.6	-	-
Qwen2.5-Omni	7B	✓	2.72	63.2	1.70	75.2	7.97	74.7
OpenAudio-s1-mini	0.5B	✓	<u>1.94</u>	55.0	1.18	68.5	23.37	64.3
IndexTTS 2	1.5B	✓	2.23	70.6	<u>1.03</u>	76.5	<u>7.12</u>	75.5
VibeVoice	1.5B	✓	3.04	68.9	1.16	74.4	-	-
HiggsAudio-v2	3B	✓	2.44	67.7	1.50	74.0	55.07	65.6
VoxCPM-Emilia	0.5B	✓	2.34	68.1	1.11	74.0	12.46	69.8
VoxCPM	0.5B	✓	1.85	72.9	0.93	<u>77.2</u>	8.87	73.0

864 F.2 EFFECT OF LM GUIDANCE ON LOCDiT
865

866 To explore CFG influence and select the best inference setting, we tested different CFG value, that
867 is, the LM (the sum of TSLM-FSQ hidden and RALM hidden) guidance on LocDiT. We found that
868 CFG value=2.0 could achieve optimal balance across all metrics. Higher weights (≥ 3.0) degraded
869 intelligibility significantly.

870 Table 8: Effect of LM guidance on LocDiT, tested on Seed-TTS-eval Benchmark.
871

872 873 CFG Value	874 EN		875 ZH		876 ZH-hard case	
	877 WER ↓	878 SIM ↑	879 CER ↓	880 SIM ↑	881 CER ↓	882 SIM ↑
875 1.0 (w/o CFG)	16.32	55.1	14.47	61.5	56.87	43.0
876 1.5	1.86	72.1	1.16	77.0	9.60	73.9
877 2.0	1.85	72.9	0.93	77.2	8.87	73.0
878 3.0	2.16	71.4	1.12	74.7	13.22	65.0
879 5.0	12.78	60.7	17.23	59.4	48.46	39.9

880
881 F.3 EFFECT OF THE SEMI-DISCRETE BOTTLENECK
882

883 This section shows more comprehensive investigation about FSQ bottleneck dimension, as shown
884 in Table 9. It can be found that when removing scalar quantization in the bottleneck layer, the
885 performance tends to degrade, showing that semi-discrete latent space maybe more stable and robust
886 than fully continuous space. Besides, we investigated the impact between FSQ and VAE regu-
887 larization as the bottleneck in VoxCPM. We replaced the FSQ bottleneck with a continuous VAE
888 bottleneck and trained it under the same setting. We specifically chose a dimension of 16 for the
889 continuous bottleneck (16d-VAE), as high-dimensional continuous latents (e.g., 256d) empirically
890 suffer from posterior collapse or inefficient compression due to optimization challenges. Under the
891 same 16-dimensional setting, the FSQ model achieves significantly better robustness than the VAE.
892 The VAE bottleneck nearly doubles the error rate on challenging cases (CER=28.17%) compared to
893 the FSQ counterpart (CER=14.42%). This confirms that the semi-discrete nature of FSQ provides
894 an indispensable inductive bias for stability that continuous regularization lacks. While the con-
895 tinuous 16d-VAE achieves slightly higher English speaker similarity than 16d-FSQ (likely because
896 continuous vectors can encode finer acoustic details), this comes at the cost of intelligibility. Our
897 default 256d-FSQ strikes the best balance, maintaining high expressivity without the optimization
898 instability associated with high-dimensional continuous bottlenecks.

899 Table 9: FSQ dimension selection study on the Emilia dataset. *Note:* The 256-dim configuration
900 was selected for the final VoxCPM configuration with the understanding that larger training datasets
901 needs more powerful modeling capabilities.

902 903 Model Setting	904 EN		905 ZH		906 ZH-hard case	
	907 WER ↓	908 SIM ↑	909 CER ↓	910 SIM ↑	911 CER ↓	912 SIM ↑
905 w FSQ: d4s9	5.18	59.3	4.05	68.0	19.55	62.3
906 w FSQ: d16s9	3.22	60.4	1.87	<u>70.5</u>	14.42	66.2
907 w FSQ: d64s9	3.22	61.1	2.14	69.8	17.48	65.1
908 w FSQ: d128s9	3.43	<u>62.2</u>	1.67	70.7	<u>16.76</u>	<u>65.7</u>
909 w FSQ: d256s9	2.98	62.6	<u>1.77</u>	70.4	18.19	64.9
910 w FSQ: d1024s9	<u>3.07</u>	62.0	2.38	69.8	20.38	64.7
911 w/o FSQ: d1024s ∞	3.67	62.1	2.30	69.6	24.92	63.5
912 w VAE: d16	3.56	62.1	1.94	69.7	28.17	62.7

913
914 F.4 EFFECT OF TRAINING PHASE ON PERFORMANCE
915

916 As mentioned in D.2, the two-phase Warmup-Stable-Decay (WSD) learning rate schedule is critical
917 for achieving optimal model performance. The initial Stable phase allows the model to converge
918 reliably to a strong baseline. The subsequent Decay phase is then essential for refining the model,

918 particularly for improving its zero-shot voice similarity capabilities. Furthermore, doubling the
 919 batch size (from 4K to 8K tokens) during the Decay phase is a necessary complement to the reduced
 920 learning rate. A larger batch size provides a more accurate and stable estimate of the gradient di-
 921 rection, which is crucial for effective and stable optimization when using very low learning rates.
 922 This strategy prevents the noise from small-batch gradients from destabilizing the fine-tuning pro-
 923 cess, enabling the model to make consistent improvements in both intelligibility (lower WER) and
 924 speaker similarity (higher SIM).

925
926 Table 10: Performance across training phases.
927

Phase	EN		ZH		ZH-Hard Case	
	WER ↓	SIM ↑	CER ↓	SIM ↑	CER ↓	SIM ↑
Stable	2.05	69.7	0.99	75.1	13.22	68.6
Decay	1.85	72.9	0.93	77.2	8.87	73.0

933
934
935 F.5 VISUAL ANALYSIS OF HIERARCHICAL REPRESENTATIONS
936

937 To validate our core hypothesis of learned implicit semantic-acoustic disentanglement, we conducted
 938 a t-SNE visualization of the internal representations in our hierarchical model. The resulting distri-
 939 butions, shown in Figures 2 and 3, empirically confirm the specialized roles of the TSLM and the
 940 RALM. Figure 2 illustrates the model’s behavior in a zero-shot voice cloning task, where each color
 941 corresponds to a distinct utterance from an unseen speaker. The TSLM-FSQ outputs form a stable,
 942 speaker-agnostic semantic-prosodic structure, while the RALM residuals cluster by speaker identity,
 943 confirming their specialized roles in content planning and acoustic refinement.

944 Figure 3 further demonstrates the VoxCPM’s capability to infer appropriate prosody and style di-
 945 rectly from text, when not using any speech prompt. When processing different text genres (news,
 946 poetry, conversation), TSLM-FSQ representations cluster by semantic category, showing that the
 947 pre-trained language model backbone effectively infers appropriate prosodic patterns directly from
 948 text content. For example, embeddings for “news” group together, separate from “story-telling”
 949 or “rap-lyrics.” The RALM outputs display greater within-category variation, indicating its role in
 950 adding fine-grained acoustic nuances to the semantic-prosodic plan.

951 To investigate whether the observed semantic-acoustic specialization originates from the hierarchical
 952 structure design or the pre-trained LLM weights, we conducted a controlled experiment. We trained
 953 a VoxCPM variant with fully random TSLM initialization and performed t-SNE visualization of its
 954 latent spaces for both zero-shot cloning (Figure 4) and text-to-speech (Figure 5) tasks.

955 The visualizations reveal that even in the absence of pre-trained semantic knowledge, the latent
 956 space exhibits a similar functional division of labor. The TSLM-FSQ hidden states still show rele-
 957 vance to semantic content and weak speaker relevance (as seen in Figure 5), while the RALM hidden
 958 states display strong speaker-dependent clustering (as seen in Figure 4). Although this self-learned
 959 specialization is slightly less distinct compared to the LLM initialized model, the consistency con-
 960 firms that the residual semi-discrete bottleneck structure itself is the key inductive bias that enables
 961 the model to self-adapt and learn a specific semantic-acoustic division of labor. The pre-trained lan-
 962 guage model parameters primarily serve to significantly sharpen, stabilize, and enhance this inherent
 963 modeling capacity.

964
965 F.6 FUSION STRATEGIES ABLATION
966

967 The LocDiT module is responsible for generating the final speech latents by conditioning on the
 968 combined semantic-acoustic representation derived from the TSLM (via FSQ) and the RALM. In
 969 the default VoxCPM configuration, we adopt a simple element-wise summation of the TSLM and
 970 RALM output hidden states as the fusion mechanism, primarily for its intuitively aligning with the
 971 “residual” nature of the design and good performance. To validate this choice, we conducted an
 972 ablation study comparing summation against several other common feature fusion strategies (con-

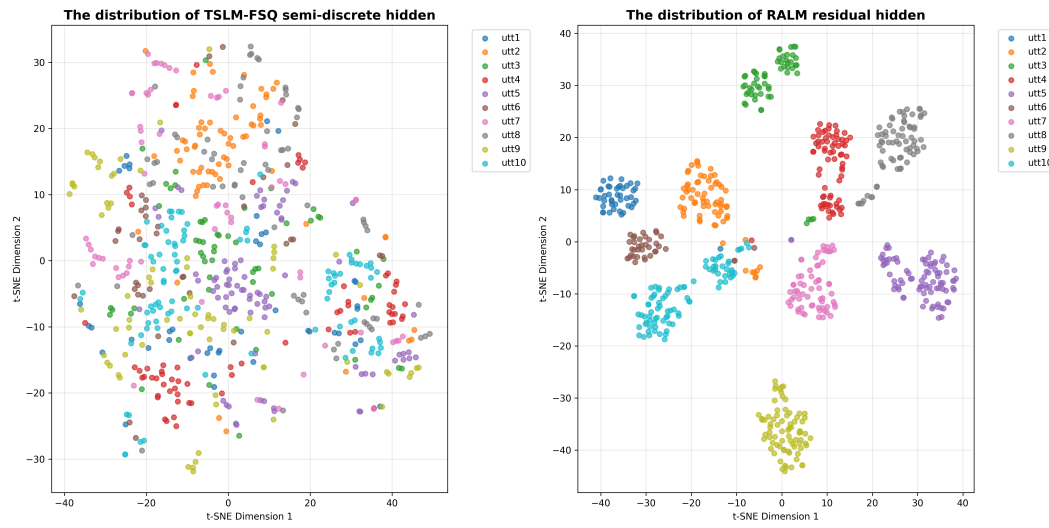


Figure 2: The T-SNE visualization of latent space distributions in zero-shot voice cloning task.

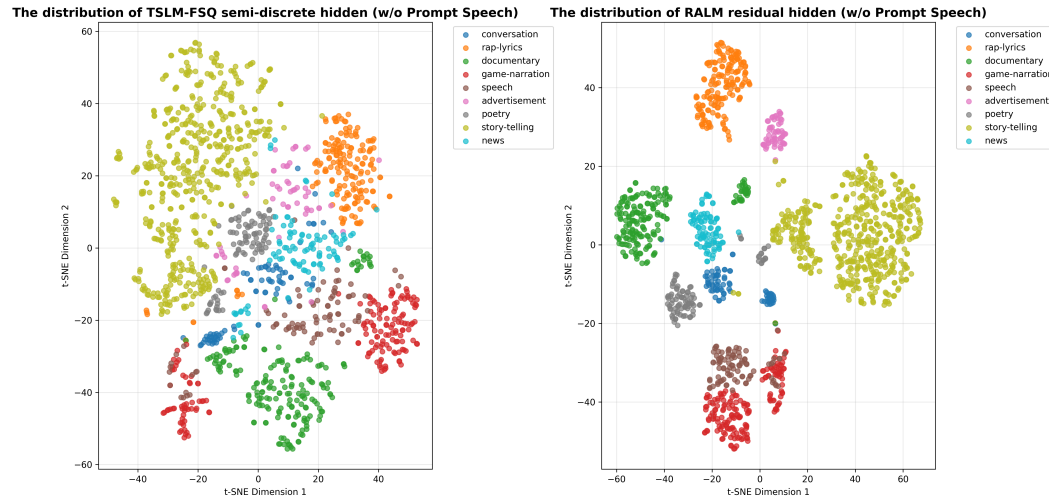


Figure 3: The T-SNE visualization of latent space distributions in text-to-speech task, without prompt speech.

catenation, gating, and attention-based fusion). The results are presented in Table 11. It shows that while **concatenation** slightly improves speaker similarity, the simple **summation** strategy achieves the best balance of intelligibility (lowest WER and CER) and acoustic quality. The significantly higher error rates observed with attention-based fusion suggest that relying on the model to dynamically learn the fusion weights introduces optimization instability in the continuous latent space.

Table 11: Ablation of different fusion strategies for combining TSLM and RALM outputs in LocDiT.

Fusion Strategy	EN-WER (↓)	EN-SIM (↑)	ZH-CER (↓)	ZH-SIM (↑)
Sum (Default)	2.98	62.6	1.77	70.4
Concatenation	3.16	64.1	2.88	71.3
Gating	3.75	63.6	2.04	70.2
Attention	4.92	59.9	5.43	66.5

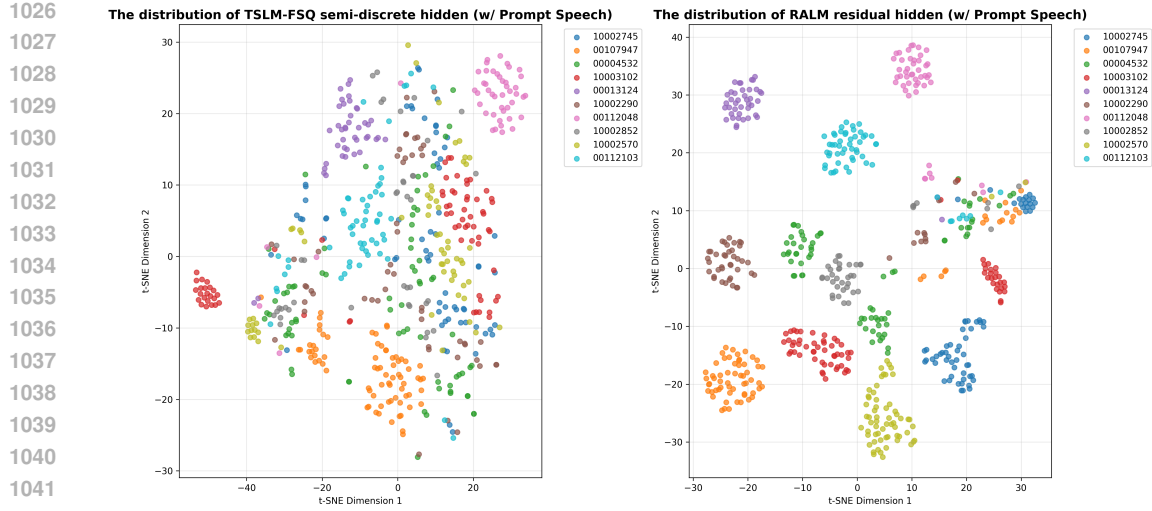


Figure 4: The T-SNE visualization of latent space distributions (without pretrained LLM parameters initialization for TSLM) in zero-shot voice cloning task.

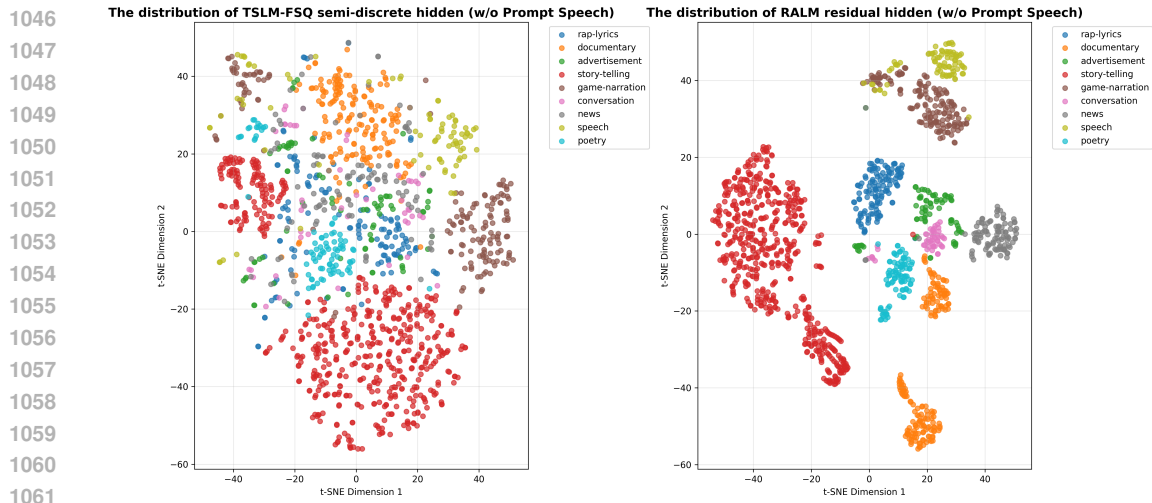


Figure 5: The T-SNE visualization of latent space distributions (without pretrained LLM parameters initialization for TSLM) in text-to-speech task, without prompt speech.

F.7 PROBING ANALYSIS FOR SEMANTIC-ACOUSTIC MODELING

To verify the core hypothesis that the FSQ bottleneck induces a functional separation of labor between the TSLM (semantic focus) and RALM (acoustic focus), we conducted **Layer-wise Probing Experiments** following the SUPERB (Yang et al., 2021) setting. We trained lightweight linear classifiers on the frozen internal hidden states extracted from four key locations: LocEnc, TSLM, FSQ, and RALM. We assessed the capture of linguistic-content using phoneme recognition (PR) and automatic speech recognition (ASR), measured by Phoneme Error Rate (PER) and WER, respectively. The lower values indicate better linguistic content preservation (higher intelligibility). Acoustic-timbre modeling was evaluated via the Automatic Speaker Verification (ASV) task, measured by Equal Error Rate (EER). The lower values indicate better speaker identity modeling (higher acoustic/timbre distinguishability).

The probing experiment results offer evidence to our core architectural claims:

- **Acoustic Features Aggregation:** The LocEnc is responsible for aggregating the low-level continuous acoustic latents from AudioVAE. Consequently, it reflects the weak semantic relevance (PER=59.12%, WER=65.79%) and carries fundamental acoustic information like timbre (EER=15.38%).
- **Semantic Specialization:** The TSLM representation achieves the lowest PER (45.60%) and WER (60.43%), validating its role in capturing the stable linguistic and prosodic content.
- **Acoustic Filtering:** The FSQ representation exhibits the highest EER (19.25%). This is a critical finding: the quantization bottleneck effectively acts as an acoustic filter, actively reducing correlation with speaker identity and prioritizing content-prosodic stability.
- **Residual Recovery:** Conversely, the RALM representation achieves the lowest EER (13.24%). This conclusively proves that the RALM specializes in recovering the fine-grained acoustic residuals and speaker identity that were filtered by the FSQ.

The slight rise in content error post-FSQ (PER=50.90%, WER=62.37%) confirms the expected lossy nature of quantization and the subsequent shift in the RALM’s focus from pure semantic modeling toward acoustic refinement. These findings empirically validate our premise: VoxCPM successfully enforces a natural division of labor using the FSQ as an inductive bias.

Table 12: Layer-wise probing results on internal hidden states of VoxCPM.

Hidden State Location	PR (PER) ↓	ASR (WER) ↓	ASV (EER) ↓
LocEnc output	59.12	65.79	15.38
TSLM last hidden (Pre-FSQ)	45.60	60.43	18.70
FSQ output	50.90	62.37	19.25
RALM last hidden	53.49	64.85	13.24

F.8 EFFECT OF MODEL SCALABILITY

We conducted a model scalability analysis to empirically demonstrate the robustness of the hierarchical VoxCPM architecture across varying capacities. We trained larger variants of VoxCPM, namely 1B and 3B parameters, on the Emilia dataset for 200k iterations.

The specific architectural configurations used for the larger models were as follows:

- **VoxCPM-1B:** This model consisted of a 28-layer TSLM ($h = 2048$), a 7-layer RALM ($h = 2048$), and 6 layers for both the LocEnc and LocDiT modules ($h = 1024$).
- **VoxCPM-3B:** This model was configured with a 32-layer TSLM ($h = 2560$), an 8-layer RALM ($h = 2560$), and 8 layers for both LocEnc and LocDiT ($h = 1024$).

As shown in Table 13, increasing the model capacity consistently improved performance across all core metrics (EN-WER, EN-SIM, ZH-CER, and ZH-SIM). Specifically, the 3B variant achieved the best intelligibility (2.60% WER) and speaker similarity (66.7% SIM). This validates that the multi-component, hierarchical design of VoxCPM remains fully scalable and effectively leverages increased parameter counts.

Table 13: Scalability analysis of VoxCPM variants trained on the Emilia dataset.

Model Size	EN		ZH	
	WER ↓	SIM ↑	CER ↓	SIM ↑
0.5B	2.98	62.6	1.77	70.4
1B	2.95	65.9	1.82	72.0
3B	2.60	66.7	1.78	72.3

1134
1135

F.9 THE COMPARISON OF REAL-TIME FACTOR AND STREAMING SYNTHESIS DETAILS

1136
1137
1138
1139

We evaluated the Real-Time Factor (RTF) of VoxCPM in comparison to other TTS models on a single NVIDIA RTX 4090 GPU. VoxCPM achieves a remarkably low RTF of 0.17, significantly faster than CosyVoice2 (0.52) and SparkTTS (0.80), due to its efficient 12.5 Hz token rate and lightweight components. The throughput for the LM backbone in VoxCPM is approximately 73 tokens/s.

1140

Table 14: The Real-Time Factor of some TTS systems.

1142
1143
1144
1145
1146
1147

TTS System	RTF ↓
CosyVoice 2	0.52
SparkTTS	0.80
IndexTTS 2	0.85
VoxCPM	0.17

1149
1150
1151
1152

Furthermore, VoxCPM supports true streaming synthesis with a theoretical first-packet latency below 100 ms: the LocDiT generates patches in under 10ms with 10 iterations, owing to its short local context and lightweight parameters, while the causal AudioVAE enables incremental processing. To ensure smooth playback, the last three latents are buffered, resulting in 80 ms audio chunks per step.

1153

G FURTHER DISCUSSION

1157

G.1 THEORETICAL GROUNDING: INFORMATION BOTTLENECK PRINCIPLES

1159
1160
1161
1162
1163
1164
1165
1166
1167

To better explain the success use of FSQ bottleneck in VoxCPM, we provide an intuitive theoretical grounding information bottleneck principles: The FSQ layer functions as a capacity-constrained bottleneck between the high-capacity TSLM and the downstream RALM. Mathematically, the scalar quantization inherent in FSQ acts as a lossy compression filter. To minimize the end-to-end diffusion loss, the TSLM is heavily penalized if it attempts to encode high-variance, fine-grained acoustic details (like timbre or specific residuals), as these would be significantly distorted by the scalar quantization step. Consequently, the TSLM is naturally forced to prioritize encoding low-variance, stable features—namely, the semantic and global prosodic structure (content, intonation). This mechanism effectively offloads the task of modeling high-frequency, complex acoustic residuals to the RALM.

1167
1168
1169
1170
1171

Empirical results from our probing experiments (Appendix F.7) validate this induced division of labor: TSLM representations demonstrate relatively high semantic accuracy (low PER and WER) but are acoustic-agnostic (high speaker EER), while RALM exhibits the opposite behavior. This confirms the FSQ's effectiveness as an internal inductive bias for hierarchical task separation.

1172

6.3 ANALYSIS ON QUANTIZATION CELL INC.

1175
1176
1177
1178
1179
1180

Continuous Latents vs. Discrete Codebooks: Discrete tokenizers like S3Tokenizer map speech signals to a fixed, finite codebook of size K , imposing a rigid, finite ceiling on expressive information (the “quantization ceiling”). Our AudioVAE operates in a 64-dimensional continuous latent space, which retains significantly richer acoustic detail and avoids the critical precision loss inherent in mapping to a finite, low-dimensional set.

1180
1181
1182
1183
1184
1185
1186

Internal FSQ Bottleneck Capacity: Inside VoxCPM, the FSQ bottleneck serves as a regularizer, not a prediction target for a small codebook. We use a high-dimensional FSQ (e.g., d256s9), offering a vast representational space far exceeding traditional VQ/FSQ codebooks. Our FSQ ablation study (Table 9) shows that when we constrain the FSQ capacity to mimic a traditional small codebook (e.g., FSQ d4s9, equivalent to 6561 vocab), the clone similarity (SIM) significantly degrades, proving that full information preservation is essential for the model’s performance ceiling.

1187

VAE Reconstruction Quality: To quantify the potential information bottleneck imposed by the VAE, we evaluated its reconstruction quality on the SEED-TTS-Eval dataset. The VAE is designed

1188 to be reconstruction-oriented with a low KL-penalty, ensuring maximum information retention. As
 1189 shown in Table 15, the VAE-reconstructed audio exhibits high fidelity across objective metrics. The
 1190 minor difference between the Ground Truth (GT) and Reconstruction confirms that the continuous
 1191 latent space effectively preserves necessary acoustic detail, distinguishing it from the significant
 1192 information loss typically associated with low-bitrate discrete tokenizers.

1193
 1194 Table 15: AudioVAE reconstruction performance comparison against Ground Truth (GT) on SEED-
 1195 TTS-Eval.

Metric	Mel Loss (↓)	STOI (↑)	WER (↓)	SIM (↑)	DNSMOS (↑)
GT	0.000	1.000	1.21	75.5	3.96
Recon	0.924	0.948	1.33	73.6	3.92

1202 H EVALUATION METRICS AND QUESTIONNAIRES

1203
 1204 To ensure robust subjective evaluation, we developed an automated interface for assessing gener-
 1205 ated speech samples. For each evaluation item, participants interact with three components: the
 1206 Evaluation Interface (containing the audio sample to be rated), the Questionnaire, and the Rating
 1207 Guidelines. Evaluations were conducted by 20 people for both English and Chinese samples.

1209 H.1 NATURALNESS MOS

1210 **Evaluation Interface:** A single audio clip accompanied by its corresponding text prompt.

1211 **Questionnaire:** To what extent does the speech sound natural and human-like? Does it convey en-
 1212 gagement with the content, or does it resemble an artificial voice lacking contextual understanding?

1213 **Rating Guidelines:**

- 1216 • 5: Indistinguishable from human speech, highly natural and engaging.
- 1217 • 4: Surpasses expectations for synthetic speech, very human-like.
- 1218 • 3: Meets expectations for AI-generated speech, reasonably natural.
- 1219 • 2: Below average, with noticeable artificial qualities.
- 1220 • 1: Clearly synthetic, lacking human-like expression.

1223 H.2 SPEAKER SIMILARITY MOS

1224 **Evaluation Interface:** A reference audio clip alongside the audio clip to be evaluated.

1225 **Questionnaire:** Focusing solely on voice characteristics (disregarding content and audio quality),
 1226 how closely does the evaluated voice match the reference voice?

1227 **Rating Guidelines:**

- 1228 • 5: Nearly identical to the reference voice, as if spoken by the same person.
- 1229 • 4: Highly similar to the reference voice, with minor differences.
- 1230 • 3: Moderately similar, sharing some vocal traits.
- 1231 • 2: Largely dissimilar, with few shared characteristics.
- 1232 • 1: Completely distinct, bearing no resemblance to the reference voice.